Current Journal of Applied Science and Technology

39(24): 66-78, 2020; Article no.CJAST.59529
ISSN: 2457-1024
(Past name: British Journal of Applied Science & Technology, Past ISSN: 2231-0843, NLM ID: 101664541)

Study and Analytical Modeling of the Influence of Technological and Geometric Parameters on the Performance of $Ga_{0.67}In_{0.33}P/GaAs/Ga_{0.70}In_{0.30}As$ Tri-junction Photovoltaic Solar Cells

N. Ndorere[1,2*], B. Kounouhewa[2] and M. B. Agbomahena[3]

[1] *Institut de Mathématiques et de Sciences Physiques (IMSP-UAC), Université d'Abomey-Calavi (UAC), 01BP 526 Cotonou, Benin.*

[2] *Laboratoire de Physique du Rayonnement (LPR-UAC), Université d'Abomey-Calavi (UAC), 01BP 526 Cotonou, Benin.*

[3] *Laboratoire de Caractérisation Thermophysique des Matériaux et Appropriation Energétique (Labo CTMA-UAC), Université d'Abomey-Calavi (UAC), 01BP 526 Cotonou, Benin.*

Authors' contributions

This work was carried out in collaboration among all the authors. Author NN designed the study, developed the analytical model used, performed simulations using Matlab software, and wrote the first version of the manuscript. Authors BK and MBA made significant contributions as supervisors, particularly in the analysis of the results and in the corrections of the Manuscript. All authors have read and approved the final manuscript.

Article Information

DOI: 10.9734/CJAST/2020/v39i2430874
Editor(s):
(1) Dr. Santiago Silvestre, Universitat Politcnica de Cataluny, Spain.
Reviewers:
(1) Munish Manas, Central University of Haryana, India.
(2) Mário Edson Santos de Sousa, Universidade Federal do Pará, Brasil.
Complete Peer review History: http://www.sdiarticle4.com/review-history/59529

Original Research Article

Received 28 May 2020
Accepted 04 August 2020
Published 20 August 2020

ABSTRACT

In the context of global energy consumption, the production of photovoltaic solar energy remains very low. One solution to this problem is to use multi-junction solar cells with high efficiency. Efforts are being made to increase the efficiency of solar cells and reduce their cost of production. In order to optimize the performance of multi-junction solar cells, this paper presents an analytical model allowing to study and model the influence of technological and geometric parameters on the performance of tri-junction solar cells $Ga_{0.67}In_{0.33}P/GaAs/Ga_{0.70}In_{0.30}As$. These parameters are the thickness, doping and Gap energy of the three sub-cells making up the tri-junction solar structure. The thicknesses and doping of the emitters (bases) of the sub-cells are varied and

**Corresponding E-mail: ndoreregity@gmail.com;*

chosen in order to optimize the efficiency of the Trijunction Solar Cell (TJSC) $Ga_{0.67}In_{0.33}P/GaAs/Ga_{0.70}In_{0.30}As$. The one hand, the base doping (emitter) is selected so as to minimize the dark current and the other hand,to reduce the resistive losses in this region. As for the thickness, it is chosen so as to minimize the recombination phenomena.
The simulation results show that for a given thickness, the sub-cell efficiencies have maximums which evolve with the increase in doping. If the doping of the base (or emitter) of the sub-cells increases, there follows a proportional increase in the efficiency. In addition, when the optimal doping and thickness of the bases (or emitters) are reached, above these, they can vary over a wide range without considerably modifying the efficiency of the solar cell. This point about the tolerance ranges is very important for the practical realization of Photovoltaic solar cell structures. These results also show that the optimal performance of the Tri-junction Solar Cell are obtained for the relatively low thicknesses of the bases (or emitters) (100nm-700nm) with high doping values $(Nb = 8e + 18cm^{-3})$ et $(Ne = 10^{19}cm^{-3})$. These optimal thicknesses are smaller than the optical penetration depths and the diffusion lengths of GaInP, GaAs and GaInAs materials.

Keywords: Tri-junction solar cell; Doping; thickeness; emitter; base.

1 INTRODUCTION

Photovoltaic solar energy has become one of the most important sources which replaces fossil energy thanks to its abundance. The large-scale use of photovoltaics is becoming more and more a reality. Small-scale electrical systems (10 - 20kW) using Silicon solar cells now compete with fossil fuel electric generators for areas isolated from conventional electrical grids [1]. The total global energy production from solar cells was $0.3GWh$ in 2000, $12.6TWh$ in 2008 and $585TWh$ in 2018 according to the International Energy Agency (IEA-2018). In 2000, production was mainly based on silicon solar cells. In 20 years, silicon solar cells have reached efficiencies above 20% and the cost has been reduced to less than $\$10/W$[2]. However, in the context of global energy consumption, the production of photovoltaic solar energy remains very low. One solution to this problem is to use high efficiency multi-junction solar cells. Efforts are being made to increase the efficiency of solar cells and reduce their cost of production. It is in this context that researchers from the National Renewable Energy Laboratory (NREL) started working on the tandem $GaInP/GaAs$ solar cell a few years ago [3-4].The cell consists of a $Ga_xIn_{1-x}P$ top sub-cell (with a band gap of $1.8 - 1.9eV$) and a bottom sub-cell GaAs (1.42eV). These sub-cells are separated by a suitable lattice interconnection tunnel junction. Before that, several groups were working on tandem device designs which should reach the theoretically efficiencies approaching $36 - 40\%$ [2-5]. In 1990, efficiencies greater than 27% for the air mass (AM1.5G) and one sun, have been achieved by modifying the thickness of the top cell for obtain a current match [6]. This adjustment of the thickness of the top cell can also be used to obtain a current correspondence under different solar spectra, for example, $AM0$ and $AM1.5D$. By using this characteristic of the tandem solar cell $GaInP/GaA$, NREL, has established the efficiency record of 29.5% [7] at $AM1.5G$. Meanwhile, many laboratories around the world were studying this device, and the record of 29.5% was finally overshadowed by researchers from the Japan Energy Corporation with the efficiency of 30.3% [8]. In order to improve the performance of multi-junction solar cells, this paper focuses on the study and modeling of the influence of technological and geometric parameters on the performance of tri-junction solar cell $Ga_{0.67}In_{0.33}P/GaAs/Ga_{0.70}In_{0.30}As$. This cell is made up of sub-cells composed of III-V semiconductor alloys. The materials $Ga_{0.67}In_{0.33}P$, with a band gap of $1.93eV$, $GaAs$, with $Eg = 1.42eV$ and the $Ga_{0.70}In_{0.30}As$, with $Eg = 1.00eV$ are particularly important examples for our case. Both n- and p-type doping of these materials are generally straightforward, and complex structures made from these materials can be grown with extremely high crystalline and optoelectronic quality by existing growth techniques. The modeling and optimization are essentially based on the parameters of the three sub-cells, namely

$Ga_{0.67}In_{0.33}P$, $GaAs$ and $Ga_{0.70}In_{0.30}As$. We are interested in the emitters and the bases of these three junctions. The parameters used are the thickness, the doping and the energy of Gap.The three sub-cells are interconnected by a tunnel junction. The thicknesses and doping of the emitters and bases of the sub-cells are varied and chosen in order to optimize the efficiency of the CSTJ $Ga_{0.67}In_{0.33}P/GaAs$ $/Ga_{0.70}In_{0.30}As$.

2 MATERIALS AND METHODS

2.1 Phenomenon of Collecting Photogenerated Carriers

In practice, the photogenerated carriers cannot all be recovered (or collected) at the terminals of the solar cell because of the recombination phenomena which exist. A solar cell is made up of an absorber and two semi-permeable membranes, one to electrons and the other to holes [9].

The semi-permeable electron membrane is the emitter, it is an n-type doped layer and that of the holes is the absorber which is a p-type doped layer and the membrane which passes the holes is the back contact of the absorber. At the interface between the emitter (type n) and the absorber (type p), a $p-n$ junction is created. The creation of this junction $p-n$ is accompanied by the creation of an internal electric field which compensates for the diffusion of carriers from each side of the junction [10]. An illustration of the $p-n$ junction is shown in Fig. 1.

When a photon is absorbed in the space charge region, the photogenerated carriers are quickly separated by strong internal electric field. The probability of collecting these carriers is therefore maximum. When a photon is absorbed in one of the quasi-neutral zones, the minority carriers (the electrons in the p-type absorber and the holes in the n-type emitter) must diffuse up to the junction in order to be collected. The characteristic distance over which the minority carriers can diffuse before recombining is the diffusion length, denoted L_n in the case of electrons and L_p in the case of holes. It is considered that carriers generated at a greater distance than L_n or L_p junction will not be collected and will be lost [11].

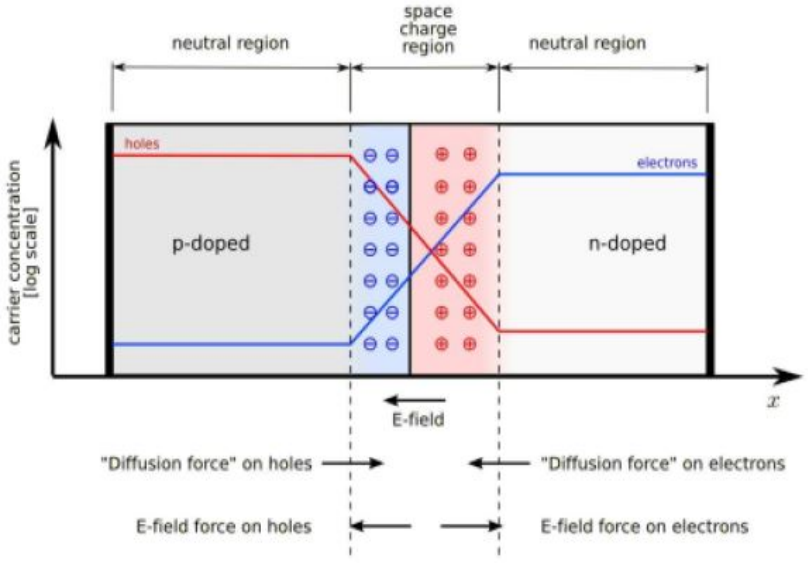

Fig. 1. Diagram of a $p-n$ junction. Contacting a p-doped zone and an n-doped zone results in the formation of a space charge zone, in which there is a strong electric field. This electric field counterbalances the diffusion of carriers on either side of the junction. We can distinguish two regions, the space charge zone and the quasi-neutral zone on either side of the junction [9]

2.2 The Choice of the Structure of the Tri-junction Solar Cell Studied

Under an AM 1.5 solar spectrum, the choice of semiconductor materials used in our work plays a very important role to obtain better efficiency. This choice mainly depends of the energy gap of these materials and their molar composition. The optimal energy gap of homojunction solar cells and which gives a better efficiency must not exceed 1.42eV as is the case for GaAs [12]. The American company Alta Devices achieves the efficiency of 28.8% for a monojunction cell made up of GaAs [13]. For monolithic tandem cells made up of two junctions, the literature gives a value between $1.75eV$ and $1.8eV$ for the top sub-cell and $1.1eV$ for the bottom sub-cell [14].

A theoretical efficiency of 36% is obtained with a tandem cell having a gap of $1.7eV$ for the top sub-cell and 1.1eV for the bottom sub-cell under the terrestrial solar spectrum AM1.5 [15-16]. The efficiency of 51.94% is obtained under the $AM1.5$ spectrum using materials with gaps $1.90eV$, $1.34eV$, and $0.94eV$ [17] and a theoretical efficiency of 53.52% is obtained under the $AM1.5$ spectrum using materials with $1.93eV$, $1.42eV$ and $1.00eV$ gaps [18]. In our case, we were inspired by ref [18] and we stacked two junctions (GaInP and GaInAs) at the optimal junction (GaAs), one top (GaInP) and the other bottom (GaInAs). The gap energy of these materials are adjusted and chosen using Vegard's law [19], by adjusting the composition of Gallium and Indium in the $Ga_xIn_{1-x}P$ and $Ga_xIn_{1-x}As$ alloys. The semiconductor materials used in tandem must have descending gaps ($(E_g1[1.93eV] > E_g2[1.42eV] > E_g3[1.00eV])$). By using these three junctions, a large part of the spectrum is absorbed and therefore more electric current is generated.

The architecture of our model cell is shown in Fig. 2. We are interested here, exclusively in the optimization of this triple junction solar cell device $Ga_xIn_{1-x}P/GaAs/Ga_xIn_{1-x}As$. Optimizing a device consists in identifying an optimal configuration, or an optimum of operation of this device. In our case, it is to determine the optimal performance of different sub-cells and to identify the parameters that impact most strongly these performances. In this perspective, we will use a parametric optimization which allows to highlight the influence of a given parameter that we want to optimize to maximize the performance of a device. In the case of optimizing the efficiency of a solar cell, this method would, for example, make it possible to know the influence of the physical, technological and geometric parameters of the cell, thus making it possible to know the optimal value of the efficiency as a function of each parameter and its sensitivity to these different parameters. The advantage of this type of optimization is the fact that the influence of each parameter on the performance of the cell is easily viewable and thus classifies these parameters according to their degree of influence.

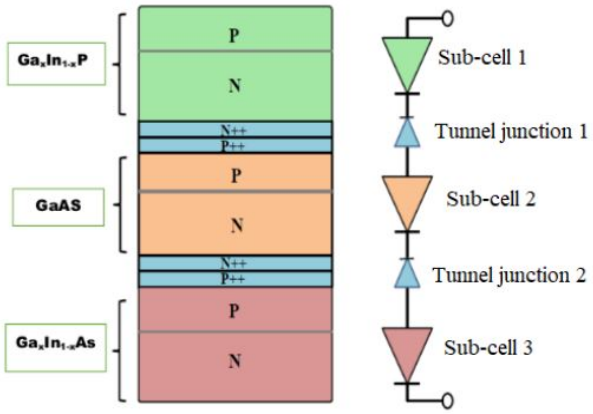

Fig. 2. Architecture of a monolithic tri-junction solar cell used in our case

2.3 Analytical Model

The analytical model is proposed to optimize and evaluate the maximum theoretical efficiency of the Tri-junction Solar Cell as a function of the technological and geometric parameters of the sub-cells that constitute it. The short circuit current density (J_{sc}) generated as a function of the band gap is calculated directly from the spectral data. The open circuit voltage (V_{oc}) is determined by the calculated short-circuit current density and the saturation current density (J_o) which depends on the parameters mentioned above[20]. The short circuit current density (J_{sc}) of each sub-cell is determined by the external quantum efficiency of the sub-cell, $QE(\lambda)$, and by the flux of photons incident on this cell $Q_{inc}(\lambda)$ as follows [21]:

$$J_{sc} = q\int_0^{\infty} \Phi_{inc}(\lambda) QE(\lambda) \mathrm{d}\lambda \tag{2.1}$$

The external quantum efficiency QE for an ideal cell of finite base thickness x_b, x_e emitter thickness and width of the space charge area W (for a total thickness $x = x_b + x_e + W$) is given by [22]:

$$QE = QE_{em} + QE_{depl} + exp\left[-\alpha\left(x_e + W\right)\right] QE_{base} \tag{2.2}$$

with

$$QE_{em} = f\alpha(L_e)\left(\frac{l_e + \alpha L_e - exp(-\alpha x_e) \times [l_e cosh(x_e/L_e) + sinh(x_e/L_e)]}{l_e sinh(x_e/L_e) + cosh(x_e/L_e)} - \alpha L_e exp(-\alpha x_e)\right) \tag{2.3}$$

$$QE_{depl} = exp(-\alpha x_e)\left[1 - exp(-\alpha W)\right] \tag{2.4}$$

$$QE_{base} = f\alpha(L_b)\left(\alpha L_b - \frac{l_b cosh(x_b/L_b) + sinh(x_b/L_b) + (\alpha L_b - l_b) exp(-\alpha x_b)}{l_b sinh(x_b/L_b) + cosh(x_b/L_b)}\right) \tag{2.5}$$

$$l_b = \frac{S_b L_b}{D_b}, l_e = \frac{S_e L_e}{D_e}, D_b = \frac{KT\mu_b}{q}, D_e = \frac{KT\mu_e}{q} \tag{2.6}$$

$$f\alpha(L) = \frac{\alpha L}{(\alpha)^2 - 1} \tag{2.7}$$

The dependence of the wavelength of photons is not explicit in these equations, but can be seen through the dependence on the wavelength of the absorption coefficient $\alpha(\lambda)$. The quantities $\mu_{b(e)}$, $L_{b(e)}$, $S_{b(e)}$ are, respectively, the mobility, the diffusion length and the surface recombination speed of the minority carriers in the base (emitter). T is the absolute temperature. In this section, we will make the simplifying assumption that each absorbed photon is converted to photocurrent, a remarkably good first approximation for high quality $III - V$ junctions. In this case, the QE very simply depends on the total thickness of the cell, $x = x_e + W + x_b$, as follows:

$$QE(\lambda) = 1 - exp\left[\alpha(\lambda) x\right] \tag{2.8}$$

because an $exp\left[\alpha(\lambda)x\right]$ fraction of the incident light is transmitted through the cell instead of being absorbed. Although equation (2.8) is obvious, it can also be deduced from equations (2.2)-(2.5) by fixing $S = 0$, $L \gg x$ and $L \gg 1/\alpha$. The incident photons Q_{inc} on the top sub-cell is simply the solar spectrum Q_s. On the other hand, the light hitting the middle sub-cell is filtered by the top sub-cell so that the middle sub-cell sees an incident spectrum $Q_s exp[\alpha_t(\lambda)x_t]$, where x_t and $\alpha_t(\lambda)$ are respectively the thickness and absorption coefficient, of the top sub-cell. Similarly, the light hitting the bottom sub-cell is filtered by the middle sub-cell and its incident spectrum is $Q_s exp[-\alpha_m(\lambda)x_m]$, where x_m and $\alpha_m(\lambda)$ are respectively thickness and absorption coefficient of the middle sub-cell.

Assuming that the bottom sub-cell is thick enough to absorb essentially all of the incident photons filtered by the middle sub-cell, we conclude that the short-circuit current densities of these three sub-cells are given by:

$$J_{sc_t} = q\int_0^{\lambda_t} \left(1 - exp\left[-\alpha_t(\lambda)x_t\right]\right)\Phi_s(\lambda)\mathrm{d}\lambda \tag{2.9}$$

$$J_{sc_m} = q\int_0^{\lambda_m} exp\left[-\alpha_t(\lambda)x_t\right]\Phi_s(\lambda)\mathrm{d}\lambda \tag{2.10}$$

$$J_{sc_b} = q\int_0^{\lambda_b} exp\left[-\alpha_m(\lambda)x_m\right]\Phi_s(\lambda)\mathrm{d}\lambda \tag{2.11}$$

where $\lambda_t = \frac{hc}{Eg_t}$, $\lambda_m = \frac{hc}{Eg_m}$ and $\lambda_b = \frac{hc}{Eg_b}$ are the wavelengths corresponding to the gap energies of the top, middle and bottom sub-cells respectively. As the middle sub-cell is filtered by the top sub-cell, J_{sc_m} depends on both Eg_m and Eg_t, while J_{sc_t} depends only on Eg_t, it is the same as J_{sc_b} which depends on Eg_m and Eg_b. In this case, $exp[-\alpha_t(\lambda)x_t] = 0$ for all photon energies greater than Eg_t and for photon energies smaller than the gap, $\alpha(\lambda) = 0$, therefore $exp[-\alpha_t(\lambda)x_t] = 1$, so that the equations (2.9), (2.10) and (2.11) become:

$$J_{sc_t} = q\int_0^{\lambda_t} \Phi_s(\lambda)\mathrm{d}\lambda \tag{2.12}$$

$$J_{sc_m} = q\int_{\lambda_t}^{\lambda_m} \Phi_s(\lambda)\mathrm{d}\lambda \tag{2.13}$$

$$J_{sc_b} = q\int_{\lambda_m}^{\lambda_b} \Phi_s(\lambda)\mathrm{d}\lambda \tag{2.14}$$

To quantitatively model the multi-junction devices, we need expressions of the curve $(J-V)$ sub-cells. For this we use the classical equations $(J-V)$ of the ideal photodiode (neglecting the regions of depletion) [22].

$$J = J_0\left[exp\left(\frac{qV}{kT}\right) - 1\right] - J_{sc} \tag{2.15}$$

where q: charge of the electron and we have assumed that the ideality factor of the diode is equal to 1. An important special case of this is:

$$V_{oc} \simeq \frac{kT}{q} ln\left(\frac{J_{sc}}{J_0}\right) \tag{2.16}$$

because in practice $J_{sc}/J_0 \gg 1$. The dark current density J_0 is given by:

$$J_0 = J_{0,base} + J_{0,em} \tag{2.17}$$

$$J_{0,base} = q\left(\frac{D_b}{L_b}\right)\left(\frac{n_i^2}{N_b}\right)\left(\frac{S_bL_b/D_b + tanh(x_b/L_b)}{S_bL_b/D_btanh(x_b/L_b) + 1}\right) \tag{2.18}$$

$$J_{0,em} = q\left(\frac{D_e}{L_e}\right)\left(\frac{n_i^2}{N_e}\right)\left(\frac{S_eL_e/D_e + tanh(x_e/L_e)}{S_eL_e/D_etanh(x_e/L_e) + 1}\right) \tag{2.19}$$

with

$${n_i}^2 = N_cN_vexp(\frac{-E_g}{kT}) = 4\left(\frac{2\pi kT}{h^2}\right)^3 {m_e}^{*\frac{3}{2}}{m_h}^{*\frac{3}{2}}exp\left(\frac{-E_g}{kT}\right) \tag{2.20}$$

where N_c and N_v are effective densities of electrons and holes, h is the Planck constant, ${m_e}^*$ and ${m_h}^*$ are effective masses of electrons and holes, E_g is the energy of the gap of the semi-conductor used.

Each junction of the multi-junction structure is described by equations (2.15) to (2.20). Equation (2.17) becomes:

$$J_0 = qn_i^2 \left[\left(\frac{D_b}{L_b N_b} \right) \frac{S_b L_b / D_b + tanh(x_b/L_b)}{S_b L_b / D_b tanh(x_b/L_b) + 1} + \left(\frac{D_e}{L_e N_e} \right) \frac{S_e L_e / D_e + tanh(x_e/L_e)}{S_e L_e / D_e tanh(x_e/L_e) + 1} \right] \quad (2.21)$$

Equation (2.21) show that V_{oc} depends on several parameters including the thickness, the doping, the diffusion lengths, the recombination coefficients etc. For the calculation of form factor (FF) and conversion efficiency (η), we use the following analytical formula [13]:

$$FF = \frac{Voc - nV_t ln\left(\frac{Voc}{nVt+0.72}\right)}{Voc + nV_t} \quad (2.22)$$

where $V_t = \frac{kT}{q}$ is the thermal voltage, k Boltzmann constant, q the elementary charge and n is the ideality factor of the cell which we can take equal to 2 at $T = 300K$. and the conversion efficiency will be calculated using the expression:

$$\eta = \frac{FF \times Voc \times Jsc}{P_{in}} \quad (2.23)$$

where P_{in} is the incident power of the $AM1.5G$ spectrum $(1000W/m^2)$. To obtain correct numerical values for the performance of Multijunction solar cells, we must choose the values of the parameters of the materials constituting the sub-cells. The diffusion lengths at $300^\circ K$ for $GaInP$ are $L_b = 3.7\mu m$, $L_e = 0.6\mu m$, for $GaAs$ are $L_b = 17\mu m$ and $L_e = 0.8\mu m$ and for $GaInAs$ are $L_b = 8.9\mu m$ and $L_e = 0.7\mu m$. For simplicity, and to give results representing the maximum possible performance, all surface recombinations are considered to be zero. In this case $S_b = 0$ and $S_e = 0$ and the equation (2.21) becomes:

$$J_0 = qn_i^2 \left[\left(\frac{D_b}{L_b N_b} \right) tanh(x_b/L_b) + \left(\frac{D_e}{L_e N_e} \right) tanh(x_e/L_e) \right] \quad (2.24)$$

3 RESULTS AND DISCUSSION

Doping and thickness play an important role in both the top and middle and bottom sub-cells. The doping of the base (emitter) is chosen so as to minimize the dark current on the one hand and to reduce the resistive losses in this region on the other hand. As for the thickness, it is chosen so as to minimize the recombination phenomena. First, we took the results corresponding to the molar fractions obtained and the gap energies of the semiconductor materials $Ga_xIn_{1-x}P$, $GaAs$ and $Ga_xIn_{1-x}As$ constituting the sub-cells of the tri-junction solar cell, which give better efficiency, as constant. Then, we varied the doping of the base (emitter) of these materials for the different thicknesses of the base (emitter) of these, in order to see their effect on the conversion efficiency (η) of these three sub-cells and of the trijunction solar cell at $300^\circ K$. The doping was varied from $10^{16} - 10^{19}$ and the thickness from $100nm - 1500nm$. Figs. 2 to 5 show the variations in the conversion efficiency (η) of the three sub-cells (top, middle and bottom) as a function of the doping of their bases (emitters) for different base (emitters) thickness values . These figures show that for a given thickness, the efficiencies of the sub-cells exhibit the maximum evolving with increasing doping.

We noted that, if the doping of the base or the emitter of the sub-cells increases, it follows a proportional increase of the efficiency until an optimum for $Nb = 8e + 18$ for the base and $Ne = 10^{19}$ for the emitter of the top sub-cell and for $Nb = 4e + 18$, $Ne = 10^{19}$ for the middle and bottom sub-cells. The same behavior is observed on the $GaInP/GaAs/GaInAs$ Tri-junction solar cell. This is explained by the increase in the open circuit voltage V_{oc} due to the decrease in the saturation current density (J_0) and the decrease in the short circuit current density due

to the increase in the resistivity of the base or the emitter.

In a second step, we looked at the optimal base (emitter) doping variation as a function of different thicknesses of the base (emitter) for all the sub-cells. We found that the efficiency increases with the decrease in the thickness of the base (emitter). For the top sub-cell for example, at an optimal base doping of $Nb = 4e + 18$, the efficiency goes from 35% to 42.5% when the thickness of the emitter is varied from $1500nm$ to $100nm$. We notice that the thickness of the emitter has a big influence on the cell efficiency compared to its thickness of the base. This situation is also observed on all the other sub-cells and on the tri-junction solar cell.

We have also noticed that when the optimal doping and thickness of the bases (or emitters) are reached, above these, they can vary over a wide range without modifying considerably the efficiency of the solar cell. This point concerning the tolerance ranges is very important for the practical realization of Photovoltaic solar cell structures. These results show that the optimal performance of Solar Cell Tri-junction are obtained for the thicknesses of the sub-cells relatively low (100nm-700nm) with high doping values $(Nb = 8e + 18cm^{-3})$ and $(Ne = 10^{19}cm^{-3})$. These optimal thicknesses are smaller than the optical penetration depths and the diffusion lengths of the materials $GaInP$, $GaAs$ and $GaInAs$.

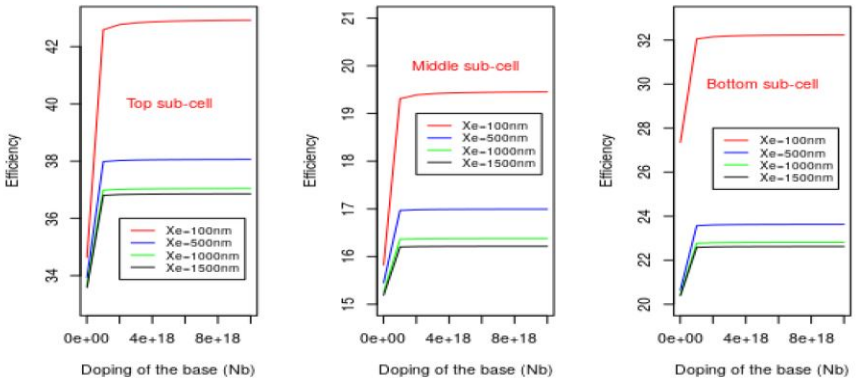

Fig. 3. Variations in the conversion efficiency (η) of the three sub-cells (Top, middle, bottom) as a function of the base doping for different values of the thicknesses of the emitter

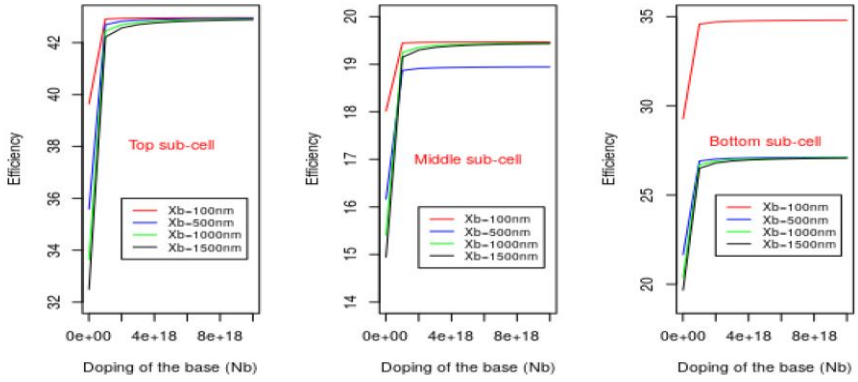

Fig. 4. Variations in the conversion efficiency (η) of the three sub-cells (Top, middle, bottom) as a function of the doping of the base for different values of the thicknesses of the base

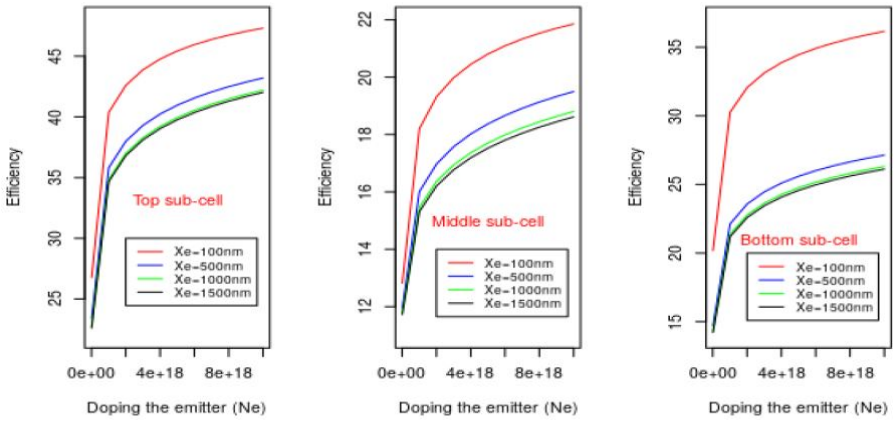

Fig. 5. Variations in the conversion efficiency (η) of the three sub-cells (Top, middle, bottom) as a function of the doping of the emitter for different values of the thicknesses of the emitter

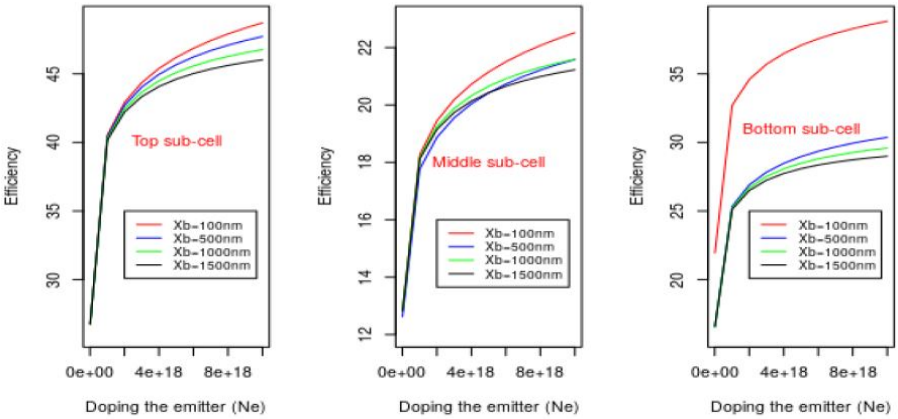

Fig. 6. Variations in the conversion efficiency (η) of the three sub-cells (Top, middle, bottom) as a function of the doping of the emitter for different values of the thicknesses of the base

In Fig. 6, we see that the effect of the thickness of the base on the efficiency of the Tri-junction Solar Cell (CSTJ) begins to be felt for very high emitter dopings $(Ne > 4e + 18)$. On the other hand in Fig. 8, we note that the effect of the thickness of the base on the efficiency of the TJSC is more pronounced for weaker dopings of the base $(Nb < 10^{18})$. The thickness of the base has no effect on the efficiency for higher doping of the base and we note that for $Nb > 6e + 18$, the efficiency of the TJSC remains constant for different values of the thickness from the base.

In Figs. 7 and 9, we see that the effect of the thickness of the emitter on the performance of the CSTJ begins to be noticed for the weaker dopings of the base or the emitter and increases as and as doping increases, but the effect is more pronounced for the thicknesses of the emitter.

Figs. 10 and 11 show the J-V characteristics of the TJSC $Ga_{0.67}In_{0.33}P/GaAs/Ga_{0.70}In_{0.30}As$. These figures are the results of the J-V characteristics of 3 sub-cells connected in series and at two terminals. The voltage at a given current for the CSTJ is equal to the sum of the voltages of 3 sub-cells which compose it, at this same current. However, in the Trijunction Solar Cell (TJSC) with sub-cells connected in series, the currents through each of the sub-

cells are forced to have the same value and it is the sub-cell that starts less current that is taken into account for the current of the CSTJ.The influence of the thicknesses and doping of the bases (or emitters) of the sub-cells on the J-V characteristics of the TJSC is shown in these graphs. We have observed that, with a strong doping $(N_{b,e} > 10^{18})$ of the base (or emitter), there follows an increase in the voltage because of the decrease in the saturation current density (J_0). But it causes a decrease in the short circuit current density because of the increase in the resistivity of the base (or emitter). In addition, the reduction in the thickness of the layers makes it possible to minimize the phenomena of recombinations in order to increase J_{sc} and V_{oc} and consequently increase the current density and the voltage of the TJSC.

Thickness and doping are two more important factors that affect the performance of solar cells.Increasing the thickness of the layers can allow a higher absorption efficiency, but not a better charge collection efficiency, which consequently limits the photovoltaic efficiency. This is due to the fact that when the material thickness is more greater than the length of charge diffusion, the probability of recombination becomes high. However, maintaining a lower layer thickness can still make it possible to minimize the recombination phenomena in order to increase J_{sc} and V_{oc}. Reasons to reduce the thickness active materials are both technological and economical. The challenge is how to increase absorption without increasing the physical thickness of the materials. In addition, doping a solar cell involves increasing its conductivity chemically. The level of doping is an important parameter for the efficiencies of multi-junction solar cells. Strong doping lowers the resistivity of the semiconductors.

In addition, the p and n doping levels on either side of the tunnel junction must allow the carriers in a band of conduction to pass by tunnel effect towards accessible states of the valence band of the adjacent cell. Indeed, the increase in doping obviously increases the electric field in the junction and at the same time causes a decrease in the space charge area (ZCE). The increase in the electric field leads to an increase in the open circuit voltage (V_{oc}). On the other hand, the decrease in the space charge area will cause a decrease in the short circuit current density (J_{sc}). These two trends of (V_{oc}) and (J_{sc}) will consequently give maximum efficiencies depending on the doping and the thickness of the emitting layers and the bases of the solar cells.

Table 1. The parameters and optimization intervals, optimal parameters and the output parameters of the three sub-cells (top, middle and bottom). The output parameters are open circuit voltage (V_{co}), short circuit current density (J_{sc}), form factor (FF) and conversion efficiency (η)

Top sub-cell	Emitter doping	Base doping	Emitter thickness	Base thickness	gallium composition
optimization parameters	$N_e(cm^{-3})$	$N_d(cm^{-3})$	$X_e(nm)$	$X_b(nm)$	x
optimization intervals	$[10^{16} - 10^{19}]$	$[10^{16} - 10^{19}]$	[100-1500]	[100-1500]	[0-1]
optimal parameters	10^{19}	8E+18	100	700	0.33
output parameters of the sub-cell		$V_{oc}[V]$	$J_{sc}[mA/cm^2]$	$FF[\%]$	$\eta[\%]$
		0.56	16.74	59.30	48.74
Middle sub-cell					
optimization intervals	$[10^{16} - 10^{19}]$	$[10^{16} - 10^{19}]$	[100-1500]	[100-1500]	[0-1]
optimal parameters	10^{19}	4E+18	100	100	-
output parameters of the sub-cell		$V_{oc}[V]$	$J_{sc}[mA/cm^2]$	$FF[\%]$	$\eta[\%]$
		0.34	14.31	44.92	22.53
Bottom sub-cell					
optimization intervals	$[10^{16} - 10^{19}]$	$[10^{16} - 10^{19}]$	[100-1500]	[100-1500]	[0-1]
optimal parameters	10^{19}	4E+18	100	400	0.30
output parameters of the sub-cell		$V_{oc}[V]$	$J_{sc}[mA/cm^2]$	$FF[\%]$	$\eta[\%]$
		0.43	18.25	49.56	31.27

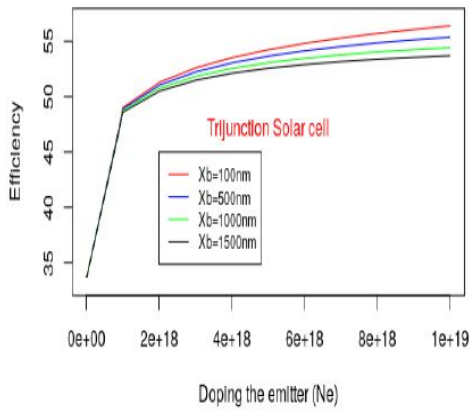

Fig. 7. Variation in the efficiency of the $Ga_{0.67}In_{0.33}P/GaAs/Ga_{0.70}In_{0.30}As$ Tri-junction solar cell as a function of the doping of the emitters of the sub-cells $Ga_{0.67}In_{0.33}P$,$GaAs$ and $Ga_{0.70}In_{0.30}As$ for different thicknesses of the bases of these sub-cells

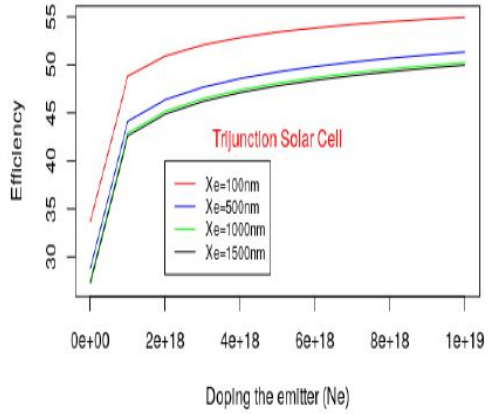

Fig. 8. Variation in the efficiency of the $Ga_{0.67}In_{0.33}P/GaAs/Ga_{0.70}In_{0.30}As$ Tri-junction solar cell as a function of the doping of the emitters of the sub-cells $Ga_{0.67}In_{0.33}P$,$GaAs$ and $Ga_{0.70}In_{0.30}As$ for different thicknesses of the emitters of these sub-cells

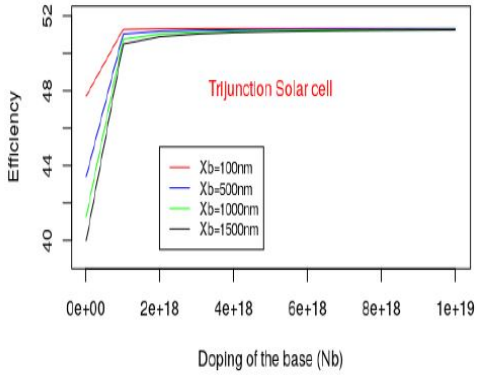

Fig. 9. Variation in the efficiency of the $Ga_{0.67}In_{0.33}P/GaAs/Ga_{0.70}In_{0.30}As$ Tri-junction solar cell as a function of the doping of the base of the $Ga_{0.67}In_{0.33}P$, $GaAs$ and $Ga_{0.70}In_{0.30}As$ sub-cells for different thicknesses of the bases of these sub-cells

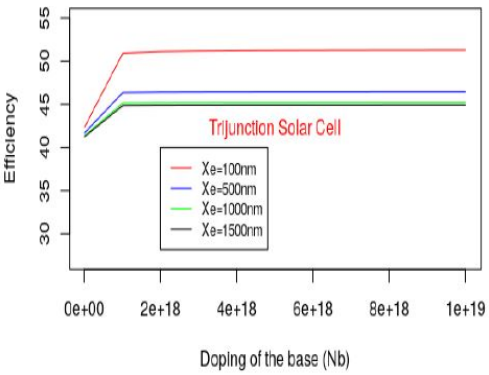

Fig. 10. Variation in the efficiency of the $Ga_{0.67}In_{0.33}P/GaAs/Ga_{0.70}In_{0.30}As$ Tri-junction solar cell as a function of the doping of the base of the $Ga_{0.67}In_{0.33}P$, $GaAs$ and $Ga_{0.70}In_{0.30}As$ sub-cells for different thicknesses of the emitters of these sub-cells

Finally, we were able to extract the optimal parameters which give maximum efficiency to three sub-cells and to the Tri-junction solar cell. These parameters are shown in Table 1. A maximum efficiency ($\eta \simeq 56\%$) of the Tri-junction solar cell is reached for the values of the following optimal parameters: the doping of the emitter ($Ne = 1e + 19cm^{-3}$), the doping of the base ($Nb \in [4e + 18 - 1e + 19cm^{-3}]$), the thickness of the emitter ($Xe = 100nm$) and the thickness of the base ($Xb \in [100 - 700nm]$).

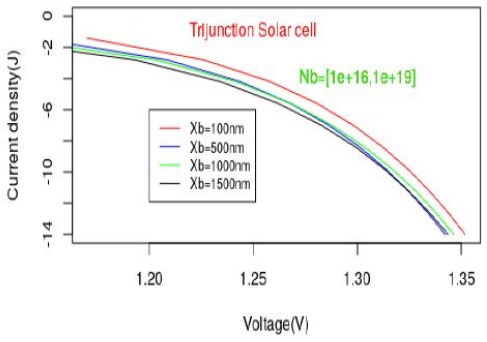

Fig. 11. Current-voltage characteristics of the Trijunction solar cell $Ga_{0.67}In_{0.33}P/GaAs/Ga_{0.70}In_{0.30}As$, taking into account the different thicknesses of the base and for a doping of the base $Nb \in [1e+16-1e+19]$

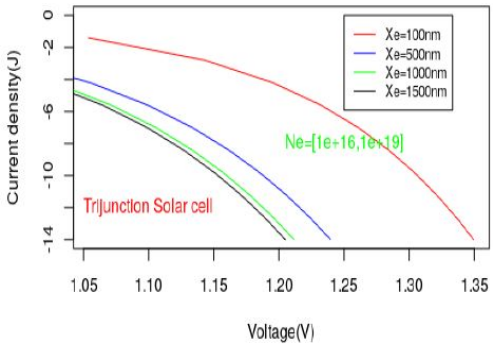

Fig. 12. Current-voltage characteristics of the Trijunction solar cell $Ga_{0.67}In_{0.33}P/GaAs/Ga_{0.70}In_{0.30}As$, taking into account the different thicknesses of the emitter and for doping of the emitter $Ne \in [1e+16-1e+19]$

4 CONCLUSION

In this work, we studied the effect of technological and geometric parameters on the performance of the $Ga_{0.67}In_{0.33}P/GaAs/Ga_{0.70}In_{0.30}As$ Tri-junction Solar cell (TJSC). We used doping parameters, the gap energy and the thickness of the GaInP GaAs and GaInAs sub-cells. We are interested in the emitters and the bases of these three junctions. The three sub-cells are connected in series and are separated by tunnel junctions. An analytical model to optimize the performance of the sub-cells based on the variation in doping and the thickness of the bases (or emitters) of these sub-cells has been developed.

The results of simulations have shown us that for a given thickness, the efficiencies of the sub-cells increase with the increase in doping up to an optimal value for which the efficiency remains fixed. In addition, the efficiencies increase with the decrease in the base (or emitter) thicknesses of the sub-cells.

Ultimately, we found that optimal performance of the Tri-junction Solar Cell are obtained for relatively low layer thicknesses $(100nm-700nm)$ with high doping values $(Nb = 8e+18cm^{-3})$ et $(Ne = 10^{19}cm^{-3})$.

These optimal thicknesses are smaller than the optical penetration depths and the diffusion lengths of the $GaInP$, $GaAs$ and $GaInAs$ materials constituting the TJSC. All these results allowed us to extract the optimal parameters which give a maximum yield to three sub-cells and the Tri-junction solar cell.

ACKNOWLEDGEMENT

The authors are grateful to the reviewers for their careful reading, constructive criticisms, comments and suggestions, which have helped us to improve this work significantly.

COMPETING INTERESTS

Authors have declared that no competing interests exist.

REFERENCES

[1] Miguel L. Contribution à l'optimisation d'un système de conversion éolien pour une unité de production isolée. Thèse de Doctorat, Université de Paris-Sud. 2008;11.

[2] Olson JM, Friedman DJ, Kurtz S. High efficiency iii-v multijunction solar cells. Handbook of photovoltaics Science and Engineering. John Wiley and Sons; 2003.

[3] Olson J, Gessert T, Al-Jassim M. Proc. 18^{th} IEEE Photovoltaic Specialists Conference. 1985;552-555.
[4] Mambrini T. Caractérisation de panneaux solaires photovoltaïques en conditions réelles d'implantation et en fonction des différentes technologies. Thèse de Doctorat, Université de Paris-Sud; 2014.
[5] Fan J, Tsaur B, Palm B. Optimal design of amorphous single-junction and tandem solar cells. Proc. 16^{th} IEEE Photovoltaic Specialist Conf. 1982;692.
[6] Kurtz S, Olson J, Kibbler A. Passivation of interfaces in high-efficiency photovoltaic devices. Appl. Phys. Lett. 1990;57:1922-1924.
[7] Bertness K, et al. Self-organized growth of regular nanometer-scale $InAs$ dots on $GaAs$. Appl. Phys. Lett. 1994;64:196.
[8] Friedman D, et al. Progress and challenges for next-generation high-efficiency multijunction solar cells. Prog. Photovolt.: Res. Appl. 1995;3:47-50.
[9] Kohen D. Étude des nanofils de silicium et de leur intégration dans des systèmes de récupération d'énergie photovoltaïque. Thèse de Doctorat, Université de Grenoble; 2012.
[10] David R. Cellules photovoltaques htrojonctions de silicium (a-Si :H/c-Si) : modlisation des dfauts et de la recombinaison linterface. Thèse,Université Paris-Saclay; 2017.
[11] Le Goff F. Intégration de matériaux semi-conducteurs III-V dans des filières de fabrication silicium avancées pour imagerie proche infrarouge. Thèse de Doctorat, Université de Strasbourg; 2017.
[12] Green M. Solar cells: Operating principles, technology and system application. Prentice- Hall, Englewood Cliffs, NJ. 1982;1-12.
[13] Writing G. Global energy assessment, toward a sustainable future 2012. Cambridge University Press; 2012. ISBN 9780521182935
[14] Brozel MR, Stillman GE. Properties fo gallium arsenides . 3rd Edition. Institution of Electrical Engineers; 1996.
[15] Dimroth F, et al. 3-6 junction photovoltaic cells for space and terrestrial concentrator applications. Conference Record of the Thirty First IEEE Photovoltaic Specialist Conference IEEE. 2005;525.
[16] Kurtz SR, Faine P, Olson JM. Modeling of two-junction, series-connected tandem solar cells using top-cell thickness as an adjustable parameter . Journal of Applied Physics. 1990;68:1890.
[17] Abdoulwahab A. Optimisation numérique de cellules solaires à très haut rendement à base d'InGaN. *Thèse de Doctorat. Université de Lorraine; 2018.*
[18] Ndorere N, Agbomahena MB, Kounouhewa B. Power efficiency analytical modeling of the tri-layer layer solar cells based on energy gap. International Journal of Current Research. 2018;10(12):76327-76338.
[19] Adachi S. Optical constants of crystalline and amorphous semiconductors numerical data and graphical information. Springer, NewYork, NY,USA; 1999.
[20] Matthias E. Nell, Allen M. Barnett. The spectral p-n junction model for tandem solar- cell design. IEEE Transactions on Electron Devices. 1987;34.
[21] Abderrezek M. Modélisation des cellules solaires tandem à couches minces et à haut rendement. Thèse, Université SETIF -1; 2015.
[22] Hovel H. Semiconductors and semimetals. Solar cells, New York.1975;11.

Peer-review history:
The peer review history for this paper can be accessed here:
http://www.sdiarticle4.com/review-history/59529